# 10. Adsorption of carbon dioxide on the clean and on the oxygen-precovered Au(110)-(1×2) surface

The final step of the catalytic CO oxidation is the desorption of the reaction product, $CO_2$. It is evident that no catalytic reaction can occur below the $CO_2$ desorption temperature, because $CO_2$ will soon occupy all available adsorption sites or, from a kinetical point of view, because a consecutive reaction cannot be faster than its slowest step. Therefore, we are interested in the temperature-dependence of the $CO_2$ desorption rate from clean gold. $CO_2$ can also adsorb on oxygen-precovered surface areas and prevent CO from getting into contact with reactive adsorbed oxygen. For this reason, also the adsorption of $CO_2$ on O/Au(110) has to be studied. The ideal method for investigating the energetics and kinetics of $CO_2$ adsorption and desorption is again thermal desorption spectroscopy (TDS). The TDS data are supplemented by results of UV photoemission and work function measurements.

## 10.1. Thermal desorption spectroscopy

Thermal desorption of $CO_2$ from Au(110)-(1×2) is characterized by several overlapping signals for mono- and multilayer desorption as illustrated in Fig. 10.1. This behaviour distinguishes $CO_2$ from the other adsorbates investigated in this work and it indicates that the $CO_2$-substrate interaction is of similar strength as the intermolecular $CO_2$-$CO_2$ interaction. Thus, adsorption and condensation may occur almost simultaneously, which can lead to a three-dimensional growth that can also make the desorption process complex. In fact, the coverage series displayed in Fig. 10.1, providing an overview over the range from 0.07 to 20.3 monolayers (ML), reveals several irregularities as for example the second-layer $\alpha$ peak appearing below the multilayer desorption temperature. The overlapping peaks and crossing curves require a somewhat unusual way of presentation (Figs. 10.2 and 10.3).

The monolayer coverage, which was achieved by an exposure of 1.32 L (at 35 K), is here defined as the maximum number of molecules in direct contact to the substrate and it corresponds to an absolute coverage[1] of $4.7\times10^{18}$ $CO_2$ molecules per $m^2$, i.e., 1.1 $CO_2$ per surface unit cell (2.89 Å × 8.16 Å). At this coverage, the $\gamma$ desorption peak is saturated (see below), the UP spectra exhibit a uniform shift of all $CO_2$ induced signals (see Section 10.2) and the work function vs. coverage curve has a bend (see Section 10.3). All these observations support our monolayer calibration. The packing density in the $CO_2$ monolayer is similar to that in the first layer of a (110)-surface of solid $CO_2$ , which contains ideally $4.45\times10^{18}$ $CO_2$ molecules per $m^2$. However, it is lower than the respective densities in $CO_2$ (100), $6.29\times10^{18}$ $m^{-2}$, and $CO_2$ (111), $7.26\times10^{18}$ $m^{-2}$.

[1] This value was determined by mass spectrometry as described in Section 4.1.6. The error amounts to 20%.

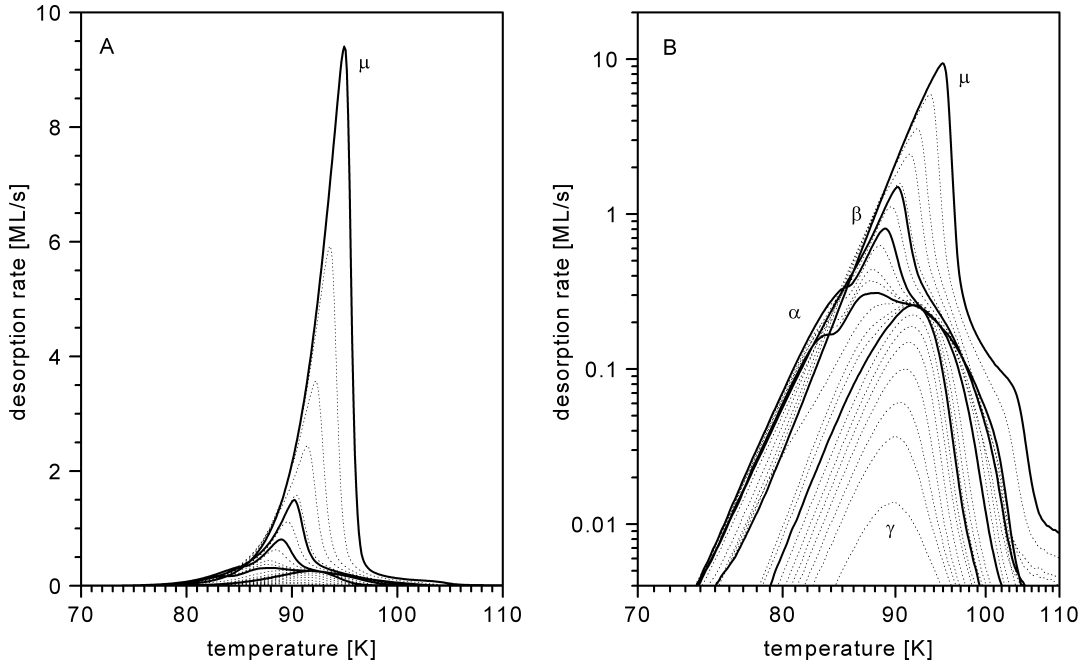


Fig. 10.1: TDS $CO_2$/Au(110)-(1×2) for coverages between 0.07 to 20.3 ML (0.09-27.0 L). Carbon dioxide ($CO_2$ gas 4.5, purity >99.995%, Messer Griesheim, Germany) was adsorbed at 35 K with a dosing pressure of $1.38\times10^{-8}$ mbar. Heating rate 2.000±0.016 K/s. The solid lines correspond to the following initial coverages (in ML): 1.00; 1.93; 3.03; 4.18, 20.3. Note the logarithmic plot in (B), which is more instructive than the linear plot (A) because of the wide dynamic range of the desorption signal.

Fig. 10.2A displays TD spectra of the $CO_2$ monolayer range ($\Theta_0 \leq 1.00$ ML, solid lines) together with higher coverage spectra (dotted lines). Desorption from the first layer is characterized by a single first-order peak, γ. A confirmation that the desorption order, n, is really close to unity is provided by the Arrhenius plot analysis displayed in Fig. 10.5.

The occurence of only *one* monolayer peak is quite remarkable if one compares with other here investigated adsorbates, which give rise to at least two sub-monolayer states with different binding energies[2]. Exceptions with only one monolayer peak are water ($H_2O$) and methanol ($CH_3OH$), which form strong intermolecular hydrogen bridge bonds. In the case of $H_2O$ desorption we also found a complete overlap of monolayer and multilayer desorption peaks. It appears evident that an adsorbate can only then discriminate between adsorption sites of different energy if there is sufficient interaction with the surface. In the cases of $CO_2$, $H_2O$, and $CH_3OH$, the intermolecular interactions apparently dominate. An interesting question which cannot be discussed here is why the saturated $CO_2$ molecule behaves on the gold surface like $H_2O$ and not, e.g., like a rare gas (cf. [Sc03] and Fig. 4.2).

[2] We found more than one desorption peak for the following adsorbates: $O_2$ (2), CO (3), $C_2H_4$ (4), Kr (3), Xe (2) (in brackets the number of monolayer desorption peaks).

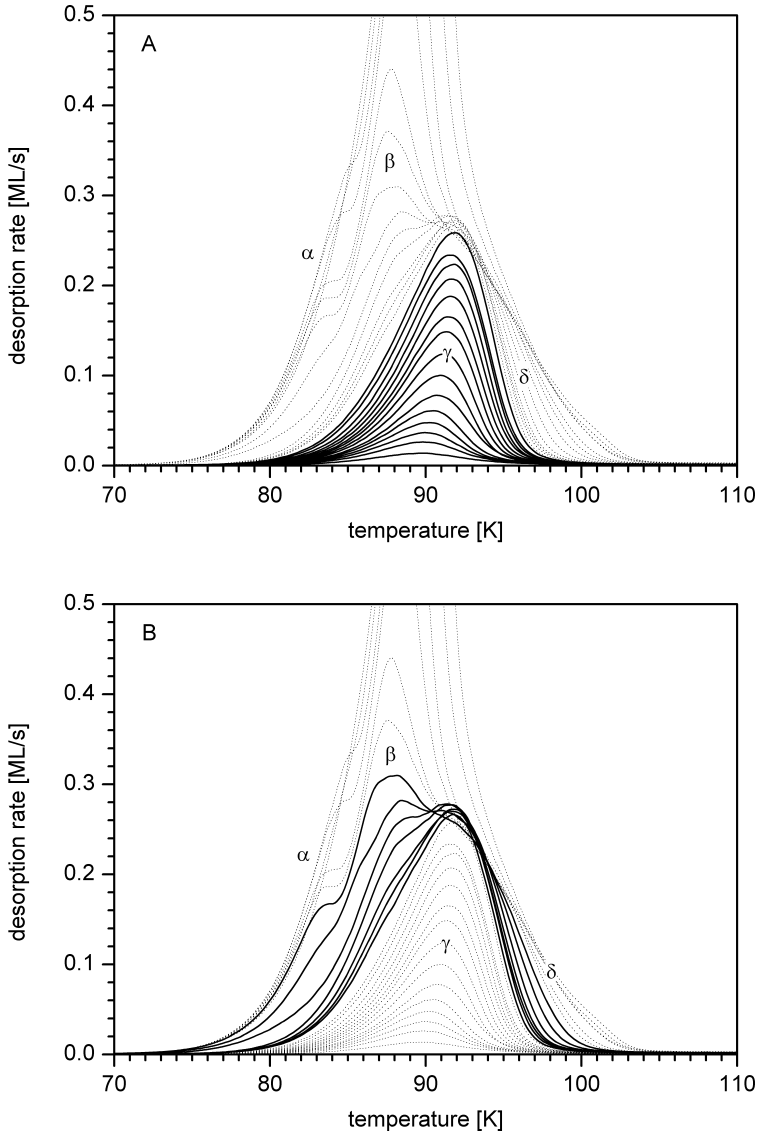


Fig. 10.2: TDS $CO_2$/Au(110)-(1×2), taken with a heating rate of 2.000±0.016 K/s. A dosage of 1.32 L afforded monolayer coverage. See Section 4.1 for the technical details of the TD experiment and caption of Fig. 10.1 for the further parameters.

(A) Monolayer range: 0.07; 0.11; 0.14; 0.17; 0.22; 0.28; 0.34; 0.42; 0.50; 0.57; 0.65; 0.73; 0.81; 0.88; 1.00 ML (solid lines).

(B) Range of 1 to 2 monolayer equivalents (MLE): 1.12; 1.19; 1.23; 1.36; 1.51; 1.72; 1.93 ML (solid lines).

The observation that the γ peak shifts to higher temperatures with increasing coverage, from 89.7 K at 0.07 ML to 91.9 K at 1.00 ML, indicates the operation of attractive interactions between the adsorbed $CO_2$ molecules. Accordingly, the desorption energy $E_{des}$, displayed in Fig. 10.4, increases by ≈ 8 % between 0.1 and 0.5 ML. The $E_{des}$ vs. $\Theta(CO_2)$ curve reaches a plateau at 0.5 ML and thus shows a similar tendency as the respective curve for $CH_3OH$/Au(110), which has a maximum at this coverage [Go01].

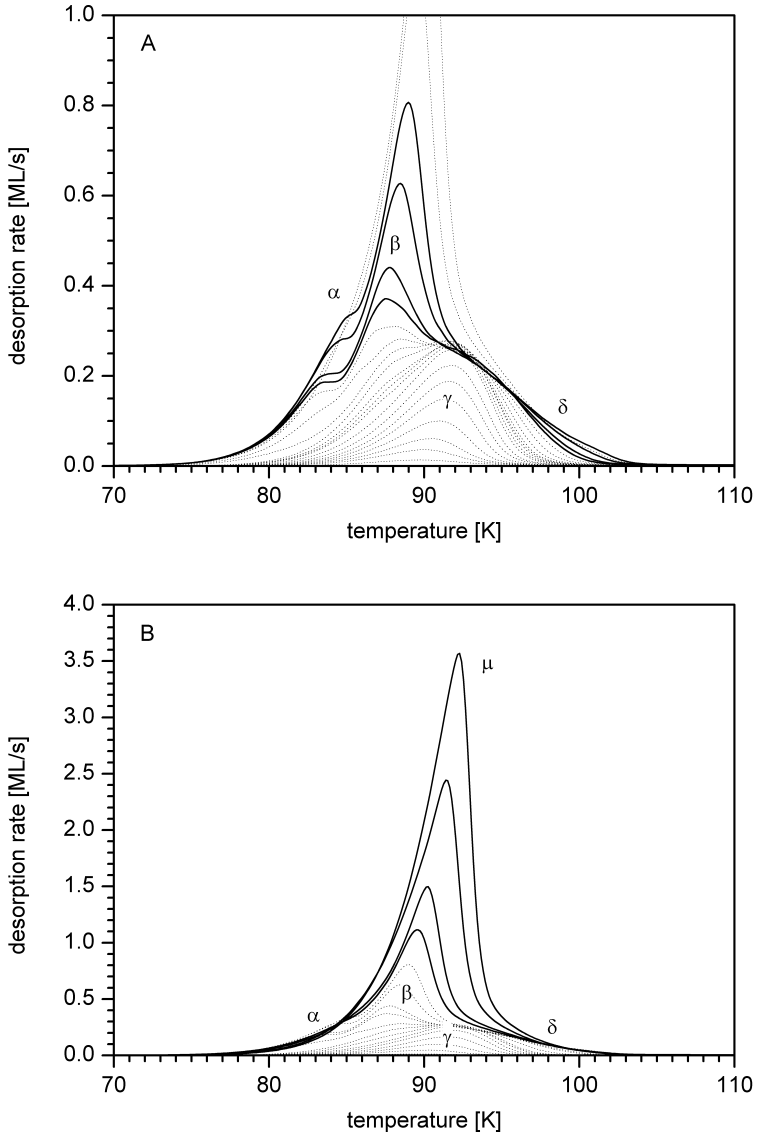


Fig. 10.3: TDS $CO_2$/Au(110)-(1×2), heating rate 2.000±0.016 K/s.
(A) Range of 2 to 3 MLE: 2.11; 2.24; 2.67; 3.03 ML (solid lines).
(B) Range of 3 to 9 MLE: 3.55; 4.19; 4.31; 6.37; 8.52 ML (solid lines).

The sticking coefficient, determined as described in Section 4.1.6, is approximately constant in the sub-monolayer range and has a value of 0.92±0.08 (see Fig. 10.6).

TDS delivers no indication of island formation in the sub-monolayer range despite the apparent attractive intermolecular $CO_2$-$CO_2$ interactions. If islands would be present, they were likely to coexist with a two-dimensional gas phase, at least around the desorption temperature. This phase equilibrium would fix the chemical potential of all phases and cause a zero-order desorption, if the sticking coefficients are approximately coverage-independent (cf. Section 4.1.4). Instead, we observe first-order desorption (Fig. 10.5).

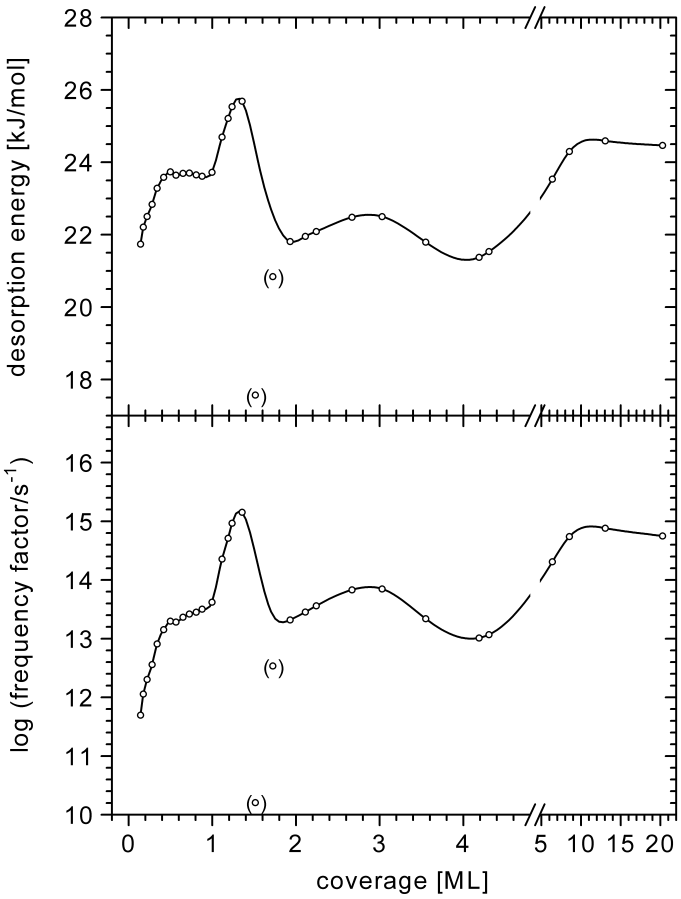


Fig. 10.4: $CO_2$/Au(110)-(1×2). Coverage-dependence of desorption activation energy and log(frequency factor) as determined by leading edge analysis (cf. Section 4.1.3). The data points in brackets are typical artefacts arising from a shoulder of a new peak falling in the analysed section and can be ignored.

Adsorption of a second monolayer equivalent[3] (MLE) leads at first to a shoulder, β, on the low-temperature side of γ. Despite the lower desorption temperature of β relative to γ, the desorption energy increases by ≈ 8 kJ/mol between 1.0 and 1.4 ML, which indicates that the interaction of a $CO_2$ molecule with a closed $CO_2$ layer is stronger than the interaction with a clean Au surface. The question arises why β desorbs at lower temperature than γ although its desorption energy is higher. An answer is provided by Fig. 10.4: the increase of $E_{des}$ is overcompensated by a parallel increase of the frequency factor.[4] As already discussed in Chapter 6, a higher frequency factor suggests a reduced (translational, rotational, or vibrational) mobility of the adparticles. The reduced mobility in the second layer could be due to the enhanced binding energy of the molecules, which restricts especially the translational motion.

[3] We prefer this expression because the following discussion shows that the formation of a closed second layer is improbable.

[4] For a discussion of the compensation effect, see Section 4.1.5.

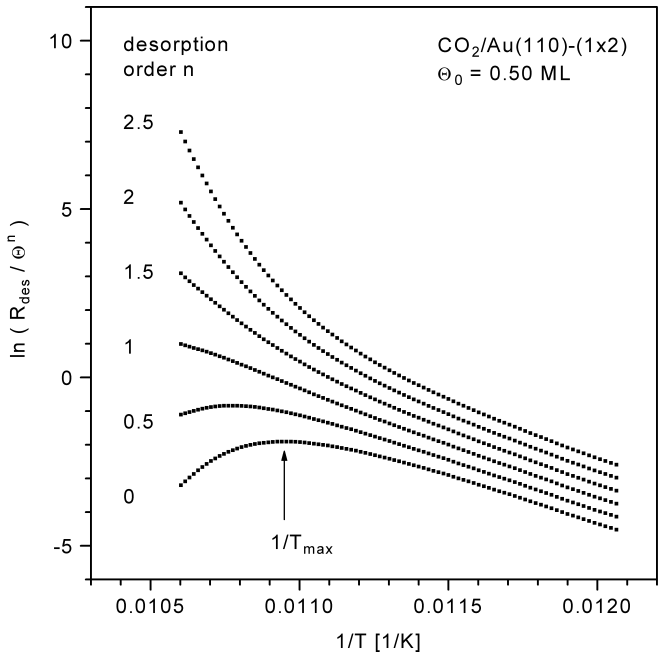


Fig. 10.5: Arrhenius plot analysis for a $CO_2$/Au(110)-(1×2) TD spectrum with an initial coverage of 0.50 ML, confirming first-order desorption in the sub-monolayer range. See Section 4.1.3 for details about this method.

Paradoxically, coverages above 1.4 ML lead to additional intensity on the low-temperature side of the β peak *and* on the high-temperature side of the γ peak. The respective shoulders are referred to as α and δ. The desorption energy (of α, since δ is not captured by the leading edge analysis) drops sharply by ≈ 4 kJ/mol (≈ 15 %) and reaches at ≈ 2 ML a value *below* the multilayer desorption energy, which is also an astonishing result. In agreement with the lower desorption energy, the α shoulder appears at lower temperatures than the multilayer peak μ, especially in the range of low rates, as Figs. 10.1B and 10.3A clearly demonstrate.

The unusual effects connected with the completion of the second layer demand an explanation: The relatively strong $CO_2$-$CO_2$ interactions, which are *not* substrate-mediated, lead above a certain coverage ($\Theta_0 > 1.4$ ML) to a 'tear-open' of the – only partially filled – second layer and to the formation of three-dimensional crystallites. The first layer apparently persists, since the γ peak is not, or only slightly, depopulated. Those finite crystallites possess, due to contributions of the surface Gibbs energy, a higher total Gibbs energy than the infinitely extended solid phase with its vanishing surface-to-volume ratio. This increase of G reduces the desorption energy (or increases the vapour pressure at fixed temperature) – a well-known phenomenon named Kelvin effect. This effect provides an explanation for the sudden desorption energy decrease and for the fact that the phase connected with α has a lower $E_{des}$ than the (more extended) multilayer phase which gives rise to the μ peak. With a reasonable estimate for the $CO_2$ surface tension (≡ the surface Gibbs energy) at the desorption temperature $T_{des}$, we are able to

derive the average size of the crystallites from the value of the desorption energy depression, which amounts to ≈ 5 kJ/mol (see below).

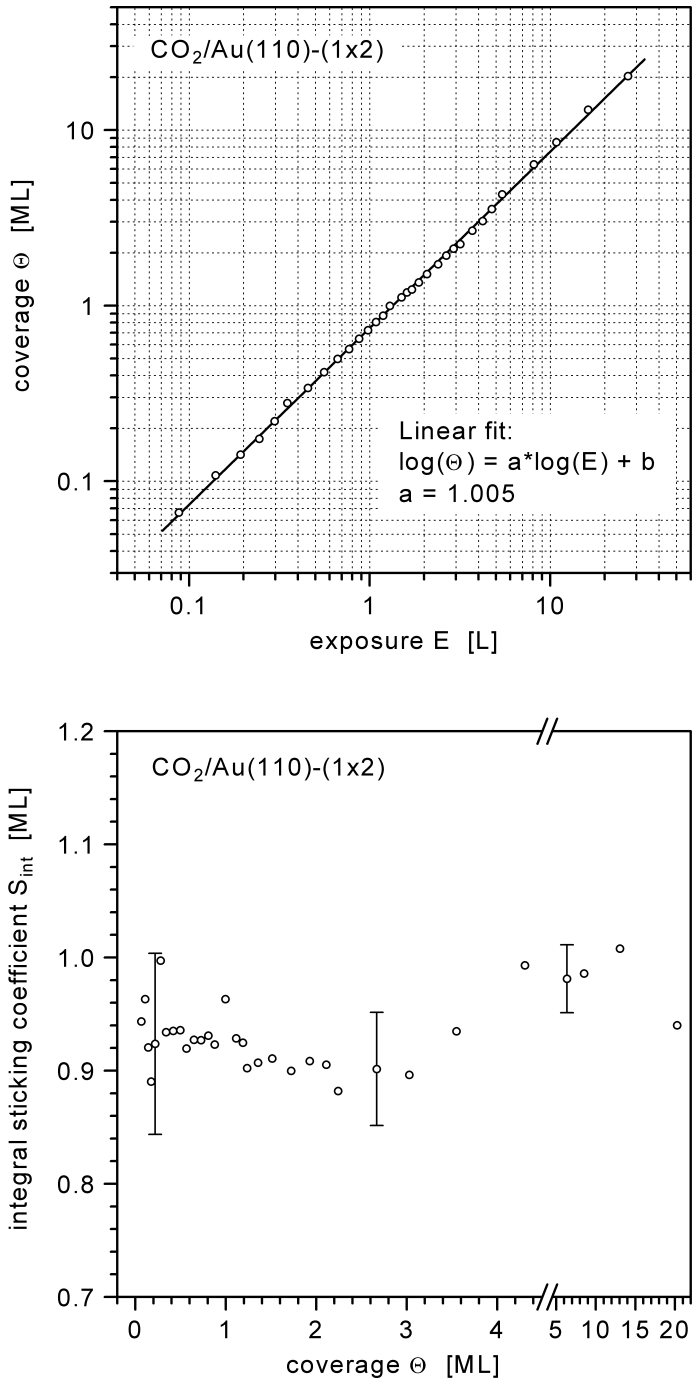


Fig. 10.6: $CO_2$/Au(110)-(1×2). $CO_2$ coverage (Θ) vs. exposure (E) and integral sticking coefficient $S_{int}$ = Θ/E for adsorption at 35 K and p($CO_2$) = 1.38×10$^{-8}$ mbar.

Furthermore, the mobility of the $CO_2$ molecules around $T_{des}$ leads to the growth of thermodynamically more stable larger crystallites on the expense of smaller ones. These larger crystallites possess still a higher energy than the extended phase – leading to a (slightly) reduced $E_{des}$ and an enhanced rate – but they exclude parts of the total coverage, namely, the molecules inside the crystallites, from the possibility to desorb. Accordingly, the desorption process is inhibited with respect to the total coverage. The crystallites act as particle reservoirs. From a certain crystallite size on this effect over-compensates the rate increase due to the Kelvin effect. The desorption peak shifts to higher temperatures and extends over a wider temperature range – which explains the additional intensity ($\delta$) on the high-temperature side of the $\gamma$ peak.

The coexistence of three desorption peaks, one of which ($\beta$) passes continuously into the multilayer desorption peak $\mu$, suggests the coexistence of layer-by-layer desorption (leading to $\beta$ and $\mu$) and desorption from three-dimensional aggregates (causing $\alpha$ and $\delta$). Provided the adsorbate undergoes no changes during heating to the desorption temperature, we can say that $CO_2$ probably prefers a Stranski-Krastanov type of growth.

In the following, we give a quantitative treatment of the preceding considerations and show that these effects can actually lead to the peculiarities observed in our thermal desorption spectra.

A. DESORPTION ENERGY DEPRESSION DUE TO THE KELVIN EFFECT – The enthalpy change, $\Delta H$, caused by a change of the surface area, $\Delta A$, is given by:

$$\Delta H = \left( \frac{\partial H}{\partial A} \right)_{p,T,n} \Delta A \,. \qquad \text{(Eq. 10.1)}$$

Eq. 10.1 contains the specific surface enthalpy, which can be derived from the surface tension, $\sigma$, and its temperature coefficient by means of the following Gibbs-Helmholtz equation:

$$\left( \frac{\partial H}{\partial A} \right)_{p,T,n} = \left( \frac{\partial G}{\partial A} \right)_{p,T,n} + T \left( \frac{\partial S}{\partial A} \right)_{p,T,n} = \sigma - T \left( \frac{\partial \sigma}{\partial T} \right)_{p,n,A} \qquad \text{(Eq. 10.2)}$$

If a spherical aggregate with radius $r_{cryst}$ changes its size by $\Delta r_{cryst}$ , $\Delta A$ amounts to:

$$\Delta A = 3V_m \, \Delta\left(\frac{1}{r_{cryst}}\right) \qquad \text{(Eq. 10.3)}$$

with the molecular volume $V_m$.

Now we consider the enthalpy change, $\Delta H$, for a transition from an infinitely extended solid ($r_{cryst} \rightarrow \infty$) to a finite spherical solid with radius $r_{cryst}$ and obtain by combining Eqs. 10.2 and 10.3:

$$\Delta H = \frac{3V_m}{r_{cryst}}\left\{\sigma - T\left(\frac{\partial\sigma}{\partial T}\right)_{p,n,A}\right\} \qquad \text{(Eq. 10.4)}$$

In order to apply Eq. 10.4 to the case of solid $CO_2$, we need the $CO_2$ surface tension $\sigma_{CO_2}(T)$, which is tabulated only for the temperature range from 221 K to 298 K [An67], and its temperature coefficient $(\partial\sigma/\partial T)_{p,n,A}$ at the desorption temperature of $\alpha$, 84 K. Extrapolation yields:

$$\sigma_{CO_2}(84K) = 71.3\frac{mJ}{m^2} \quad \text{and} \quad \left(\frac{\partial\sigma}{\partial T}\right)_{84K} = -0.527\frac{mJ}{m^2 K} \; . \qquad \text{(Eq. 10.5)}$$

Both values have to be regarded as crude estimates since (a) we extrapolate over a wide T range which includes a liquid-solid phase transition and (b) the $\sigma$ values are tabulated for the equilibrium pressure and not for $p \rightarrow 0$. Approximation (a) may lead to substantial, (b) only to minor errors. Thus, an independent estimate for $\sigma$ desirable. For this purpose, we consider that $\sigma$ is the energy expense per area for creating a surface by cleavage of a crystal. With the bulk cohesive energy, $E_{coh}$, the density of surface atoms, $N_s/A$ and the fraction of broken bonds per surface atom, $Z_s/Z$, $\sigma$ can be estimated by:

$$\sigma \approx E_{coh}\frac{N_s}{A}\frac{Z_s}{Z} \qquad \text{(Eq. 10.6)}$$

$E_{coh}$ can be approximated by the sublimation energy, $\Delta U_{subl}$, at the respective temperature. $\Delta U_{subl}(T)$ can be derived from the tabulated standard sublimation enthalpy [An67] under consideration of the heat capacities for solid and gaseous $CO_2$. We apply the sublimation energy instead of the enthalpy, because no volume (expansion) work is exchanged in a pumped system. The resulting value for 84 K is $\Delta U_{subl} = 26.38$ kJ/mol and, thus, $E_{coh} \approx 4.38\times10^{-20}$ J/particle. (We remark here that $\Delta U_{subl}$ is smaller than the multilayer

desorption energy $E_{des}(\mu)$ as displayed in Fig. 10.4, a result which suggests that the multilayer consists also of – larger – finite crystallites. However, the system is apparently even more complex. An Arrhenius plot analysis of a multilayer peak yields a desorption energy of 25.6 kJ/mol – which is closer to $\Delta U_{subl}$ than to the $E_{des}(\Theta)$ values shown in Fig. 10.4. The reason for this deviation may be an inhomogenous multilayer phase. The beginning of the leading edge, which is employed in the Habenschaden-Küppers analysis, is probably controlled by desorption of small crystallites with a reduced desorption energy, whereas the main part of the spectrum reflects desorption of an extended multilayer phase with $E_{des} \approx \Delta U_{subl}$.)

For determining $N_s/A$ and $Z_s/Z$, we have to consider the crystal structure of solid $CO_2$. The cubic $CO_2$ unit cell (5.64 Å) contains four molecules. This means, the $CO_2$ (111) as the most stable surface exposes ideally $N_s/A = 7.26\times10^{18}$ $CO_2$ molecules per $m^2$. A molecule in this surface lacks $Z_s = 3$ van-der-Waals 'bonds' from the 12 'bonds' of a bulk molecule. Thus, we obtain

$$\sigma_{CO_2} \approx 79.5 \frac{mJ}{m^2}, \qquad \text{(Eq. 10.7)}$$

which is close (within 10%) to the independently – by extrapolation – estimated value for $\sigma_{CO_2}$ (Eq. 10.5).

Applying the values given in Eq. 10.5, we obtain, with the molecular volume of $CO_2$, $V_m = 2.88\times10^{-5}$ $m^3$/mol, an enthalpy change of

$$\Delta H = 9.97\times10^4 \frac{JÅ}{mol} \times \frac{1}{r_{cryst}}. \qquad \text{(Eq. 10.8)}$$

Experimentally, we found a difference of 4.9 kJ/mol between the desorption energy of the $\alpha$ state, ≈ 21.5 kJ/mol, and $\Delta U_{subl}$. According to Eq. 10.8, this value of $\Delta H$ corresponds to a crystallite radius of $r_{cryst} = 20.3$ Å (equivalent to 733 $CO_2$ molecules per crystallite).

B. HIGH-TEMPERATURE PEAK SHIFT DUE TO A REDUCTION OF THE EFFECTIVE COVERAGE – As mentioned above, desorption of a crystallite is confined to its surface. The effective coverage, which enters the Polanyi-Wigner equation, is determined by the surface-to-volume ratio of the particle numbers, $N_s/N_v$:

$$\Theta_{eff} = \Theta_{tot} \frac{N_s}{N_v} \qquad \text{(Eq. 10.9)}$$

with the total coverage $\Theta_{tot}$.

For spherical aggregates with radius $r_{cryst}$ consisting of particles with the van-der-Waals radius $r_{vdW}$, simple geometric arguments yield for $r_{cryst} >> r_{vdW}$:

$$\frac{N_s}{N_v} = 2\sqrt{6}\,\frac{r_{vdW}}{r_{cryst}}. \qquad \text{(Eq. 10.10)}$$

Thus, the formation of crystallites leads to a decrease of the desorption rate (since $\Theta_{eff} \le \Theta_{tot}$). During desorption, the crystallites shrink and the inhibiting effect is increasingly counterbalanced by the Kelvin effect. Consideration of both effects leads, by combining Eqs. 10.4, 10.9, and 10.10, to the following modified Polanyi-Wigner equation (cf. Eq. 4.1):

$$R_{des} = \nu \exp\left\{ -E_{des} + \frac{3V_m}{r_{cryst}}\left( \sigma - T\left(\frac{\partial\sigma}{\partial T}\right)_{p,n,A} \right) \right\} 2\sqrt{6}\,\frac{r_{vdW}}{r_{cryst}}\,\Theta_{tot} \qquad \text{(Eq. 10.11)}$$

We performed a numerical integration of Eq. 10.11 for an arbitrary ensemble of crystallites with different initial sizes in order to demonstrate that the shoulders α and δ in the $CO_2$ TD spectra can indeed arise from the described effects, viz., the Kelvin effect for small and the inhibited desorption for large crystallites. We made no attempt to fully simulate the experimental TD spectra because no information about the actual size distribution of the crystallites at the desorption temperature is available. By applying the parameters for $CO_2$ as derived in the preceding sections and assuming $E_{des} = \Delta U_{subl}$ we obtained the result shown in Fig. 10.7. In the simulation, we explicitly considered the decrease of $r_{cryst}$ from the initial value, $r_{cryst,0}$, to the final value, which equals $r_{vdW}$ (single molecule), in the course of desorption. The main peak of the simulated spectrum in Fig. 10.7A arises from desorption of extended $CO_2$ multilayers ($r_{cryst,0} \rightarrow \infty$) which are assumed to contain most of the adsorbed $CO_2$ (76%). Crystallites with small initial radii ($r_{cryst,0} \le 50$ Å) lead to additional intensity at the low-temperature side of this peak. It is evident that a continuous size distribution will lead to a shoulder similar to α in the experimental spectrum in Fig. 10.7B. In contrast, for crystallites > 80 Å the inhibition of the desorption process due to the excluded-particle effect initially overcompensates the Kelvin effect. This inhibition leads to a high-temperature shift and thus to additional intensity on the high-temperature side of the main peak. At the end of desorption, the crystallites become very small and the rate increases due to the Kelvin effect, resulting in the sharp high-temperature edges arising from the contributions of 100 Å, 150 Å, and 300 Å crystallites in Fig. 10.7A. As for the small aggregates, it is easy to imagine that a continuous size distribution leads to a shoulder similar to δ in the experimental spectra.

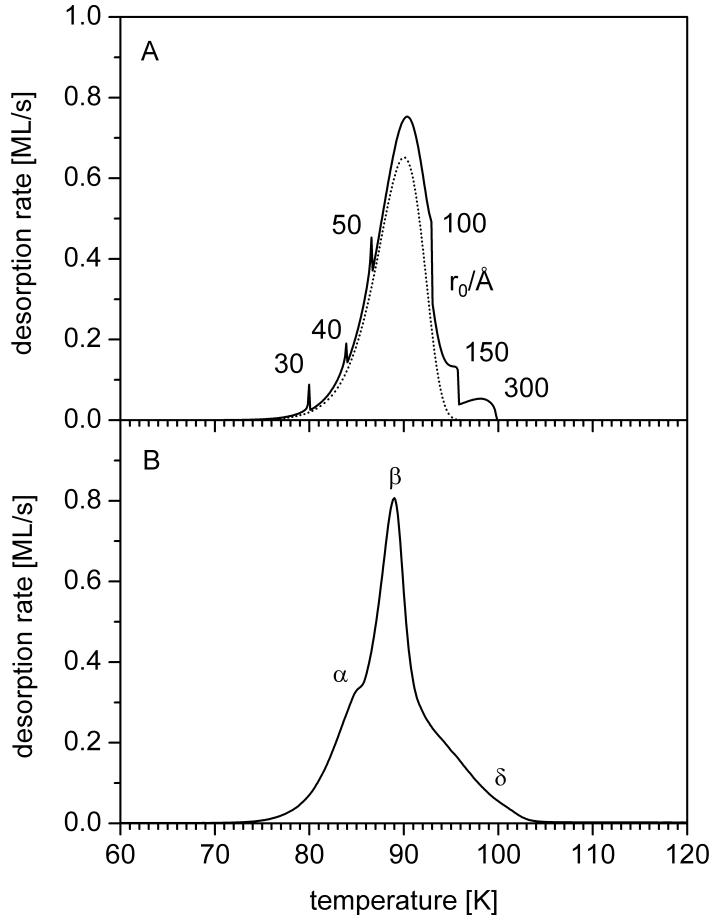


Fig. 10.7: (A) Calculated TD spectrum for desorption in the presence of a *discrete* (non-continuous) size distribution of $CO_2$ crystallites. The total coverage of 3 ML is distributed over crystallites of selected radii as follows (in % of $\Theta_{tot}$): 30 Å (0.22%), 40 Å (0.65%), 50 Å (1.3%), 100 Å (8.7%), 150 Å (7.6%), 300 Å (5.4%). The remaining 76% of $\Theta_{tot}$ are contained in extended multilayers (dotted line). Further parameters in Eq. 10.11: $E_{des} = \Delta U_{subl}$ = 26.38 kJ/mol, $\log(\nu/s^{-1})$ = 15.2, $V_m = 2.88\times10^{-5}$ $m^3$/mol, $r_{vdW}$ = 1.99 Å, $\sigma$ = 71.3 mJ/$m^2$, $(\partial\sigma/\partial T)$ = -0.527 mJ/($m^2$K). (B) Experimental spectrum (3 ML). Comparison of A and B shows that a *continuous* distributions of crystallites of different radii can lead to a TD spectrum as shown in B.

## 10.2. UV photoelectron spectroscopy

UP spectra of adsorbed $CO_2$ were measured with He-I radiation (21.22 eV). The $CO_2$ gas was dosed at a sample temperature of 28 K with a pressure of $1.38\times10^{-8}$ mbar. After the recording of each spectrum, the sample was heated to 300 K.

The resulting UP spectra for various $CO_2$ coverages are displayed in Fig. 10.8, the respective difference spectra in Fig. 10.9. The $CO_2$ induced emissions show the same energetic spacings as those of the free molecule, as comparison with the $CO_2$ gas phase UP spectrum reveals. The lack of differential peak shifts reflects the weak $CO_2$-substrate interaction, which was also responsible for the irregular desorption behaviour observed with TDS. Coverage-dependent effects in the sub-monolayer range are restricted to a small uniform shift of all peaks by 0.15 eV between 0.6 and 1.0 ML.

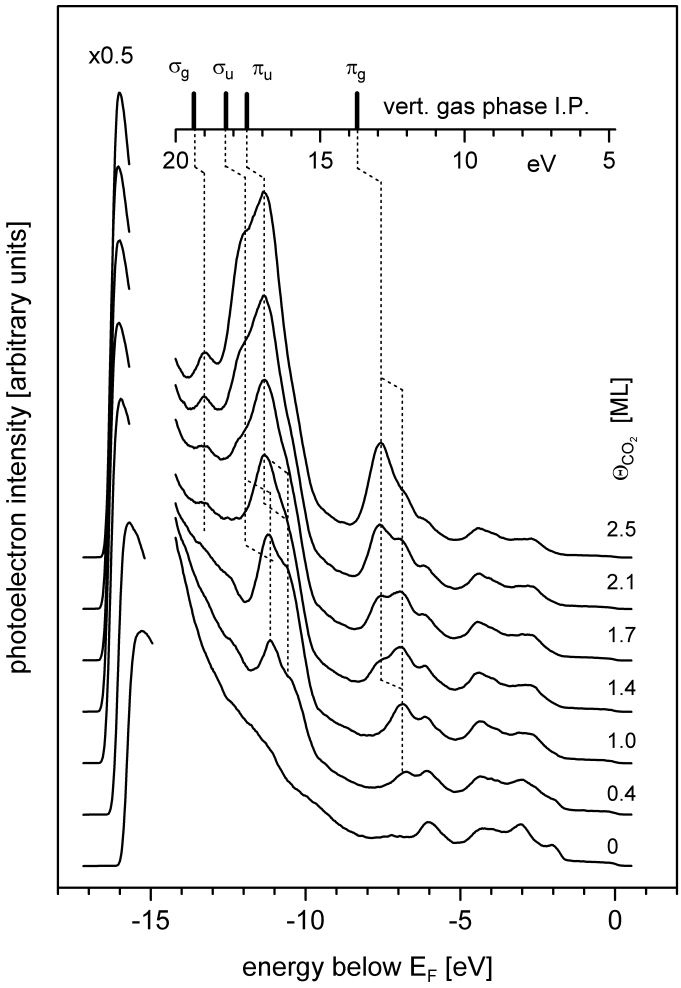


Fig. 10.8: He-I UP spectra (hν = 21.22 eV) of $CO_2$ on Au(110)-(1×2). Sample temperature 28 K, bias -10 V, normal emission, light incidence angle 60°. The gas phase values were taken from [Tu70]. The energy scales (with reference to $E_F$ and $E_{vac}$, respectively) were aligned by shifting the gas phase spectrum by $\varphi_0 + \Delta\varphi$ with $\varphi_0 = 5.37$ eV and $\Delta\varphi = -0.58$ eV for the work function change at monolayer coverage (see Section 10.3).

In contrast, the completion of the first layer and the onset of condensation is accompanied by a shift of all peaks towards higher binding energies. The origin of this shift has already been discussed in the context of the CO UP spectra (Section 8.2): the final $CO_2^+$ hole state is more effectively stabilized by the metal (metallic screening of the first layer) than by a surrounding of other molecules (dielectric screening in condensed $CO_2$). The energy gain is added to the kinetic energy of the electron and leads to a lower apparent binding energy for the electron which leaves the more stable (since better screened) ion behind. The amount of shift is 0.7 eV for $\pi_g$, 0.6 eV for $\pi_u$, and ≈ 0.8 eV for $\sigma_u$, i.e., it roughly the same for all peaks. This general relaxation shift also supports our assumption that a saturated γ peak in TDS corresponds to a completion of the first layer.

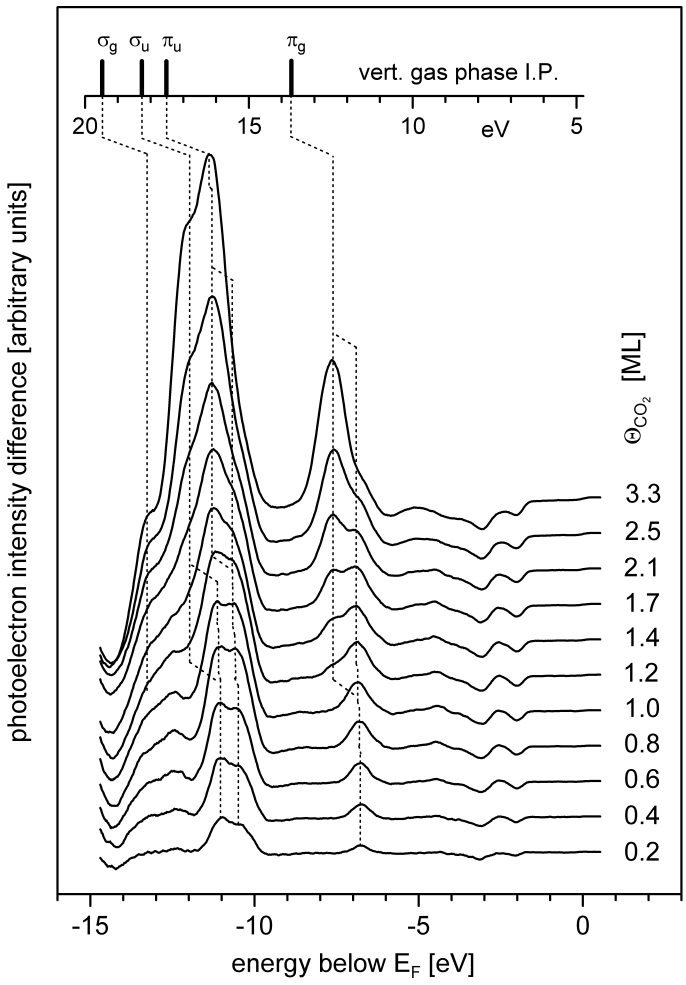


Fig. 10.9: He-I UP difference spectra of $CO_2$/Au(110)-(1×2), obtained by subtraction of a spectrum of the clean surface. See Caption of Fig. 10.8 for the other parameters.

### 10.3. Work function measurements

$CO_2$ adsorption on Au(110)-(1x2) causes a negative work function change. This is illustrated by Fig. 10.10, which additionally shows that the Δφ vs. exposure curve is relatively smooth and possesses neither the minimum/maximum structure as observed for CO nor even the sharp bends of the respective $C_2H_4$ curve. Instead, the curve reminds to that of a rare gas, e.g., krypton [Sc03]. However, consideration of the second derivative (dotted line in Fig. 10.10), which allows to determine the exact positions of the bends in the Δφ curve, reveals that the gradient changes the most at 1.32 L, an exposure that was assumed to afford monolayer coverage since it leads to saturation of the γ peak in TDS (see Section 10.1). Thus, Δφ provides a third independent support for our monolayer calibration.

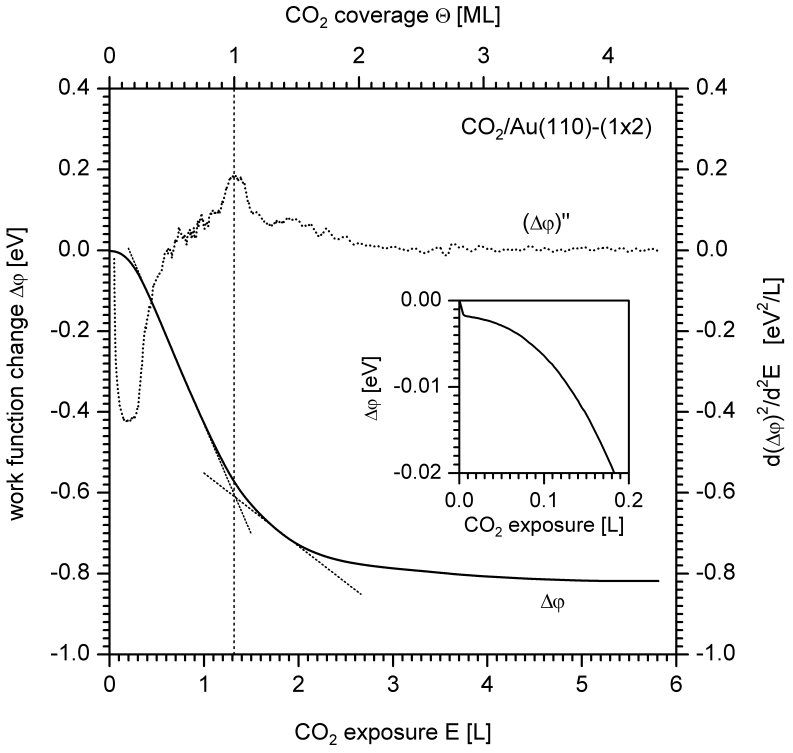


Fig. 10.10. $CO_2$ induced work function change vs. exposure and coverage upon adsorption at 28 K and $p(CO_2) = 1.38\times10^{-8}$ mbar (solid line). Exposures were converted into coverages by assuming a constant sticking coefficient for the whole coverage range. Thus, the coverage scale is only approximate, although the effective error is very small. The maximum in the second derivative (dotted line, smoothed) coincides with the completion of the first layer.

On the other hand, the fact that the work function decreases further above ML coverage suggests that three-dimensional island growth occurs parallel to the layer adsorption and that no closed first layer is formed at 28 K. Despite this fact, TDS shows only one first-order ML desorption peak, which suggests that the islands dissolve upon heating to the desorption temperature. Support for this idea is provided by temperature-dependent work function measurements. In these experiments, $CO_2$ adsorbate phases, prepared at 28 K, were heated under simultaneous work function detection. We found that the work function decreases by ≈ 90 meV between 60 K and 75 K, i.e. just below the desorption temperature. We interpret this observation as the temperature-driven dissolution of islands, a process which increases the local $CO_2$ coverage and, thus, the work function change.

The $\Delta\varphi$ vs. $\Theta(CO_2)$ curve is approximately linear between 0.25 and 0.85 ML. In this range, the Helmholtz equation (Eq. 4.48) yields a dipole moment of $|\mu_0| = (0.40 \pm 0.08)$ D for the individual adsorption complex. This value is larger than that of $O_2$-Au (because of the higher polarizability of $CO_2$), but less than half as large as the CO-Au adsorbate dipole (probably because of the lack of adsorbate/adsorbate orbital/orbital interaction in the case of $CO_2$).

## 10.4. LEED

We investigated $CO_2$ adsorbate phases on Au(110)-(1×2) from sub-monolayer to multilayer coverages with electron diffraction. In the temperature range between 28 K and 100 K we found no long-range ordered phases, a similar result as for the other adsorbates studied in this work, $O_2$ and CO. Our result is not singular, since for $CO_2$ adsorption on a congener of our surface, Cu(110), Schlatterbeck [Sc92a] and Ernst et al. [Er99] reported that no ordered structures could be observed at temperatures down to 18 K. As possible reasons, the authors suggested that the mobility of the molecules may be still high enough to prevent effective ordering or, alternatively, that the electron beam causes a disorientation of the molecules.

## 10.5. $CO_2$ adsorption on oxygen-precovered Au(110)-(1×2)

$CO_2$ adsorption on oxygen-precovered gold (O/Au(110)-(1×2)) was studied by thermal desorption spectroscopy under the same conditions as adsorption on the clean surface. The chemisorbed oxygen adlayer was prepared by electron irradiation of physisorbed $O_2$ (as described in Chapter 5) and heated to 300 K prior to the first $CO_2$ adsorption, which was performed at 30 K. The resulting $CO_2$ thermal desorption spectra for an oxygen coverage of 1.2 ML are displayed in Fig. 10.11. In the sub-monolayer range, two desorption states $\gamma_O$ ($T_{des} < 118$ K) and $\beta_O$ ($T_{des} < 109$ K, above ≈ 0.2 ML $CO_2$) can be distinguished. High dosages lead to another peak $\mu_O$ of condensed $CO_2$ around 87 K. At medium coverages (≈ 2 ... 3 ML), we again observe a shoulder, $\alpha_O$, below the desorption temperature of condensed $CO_2$ multilayers.

Oxygen-preadsorption increases the $CO_2$-substrate binding energy relative to the clean surface. This fact is illustrated by the inset in Fig. 10.11, which displays TD spectra of $CO_2$/Au (dotted line) and $CO_2$/O/Au (solid line) for $CO_2$ coverages of 0.12 and 1.0 ML. The oxygen-induced high-temperature peak shift at low $CO_2$ coverages amounts to ≈ 27 K, which is equivalent to a desorption energy increase of ≈ 7 kJ/mol (assuming $\nu = 10^{11}$ $s^{-1}$).

Furthermore, oxygen preadsorption leads to repulsive interactions between the adsorbed $CO_2$ molecules, as indicated by the low-temperature shift of the sub-monolayer TD spectra. In contrast, on the clean surface we had observed (weak) attractive interactions. Both oxygen-induced effects suggest that the $CO_2$-surface bond is predominantly electrostatic. The unpolar $CO_2$ molecule is polarized by the surface dipole – which is, on the clean surface, entirely due to the electron spill-out – and attracted by dipole/induced dipole forces. On the oxidized gold surface, the surface dipole is larger than on clean gold, as indicated by the increased work function ($\Delta\varphi \approx +1$ eV at $\Theta(O_{ad}) = 1$ ML). This more polar surface induces a larger dipole moment in the adsorbed $CO_2$ and causes an enhanced attraction to the surface. On the other hand, the larger induced dipole moment leads to increased repulsive electrostatic adsorbate/adsorbate interactions – which explains why repulsion is seen in the $CO_2$/O/Au, but not in the $CO_2$/Au spectra.

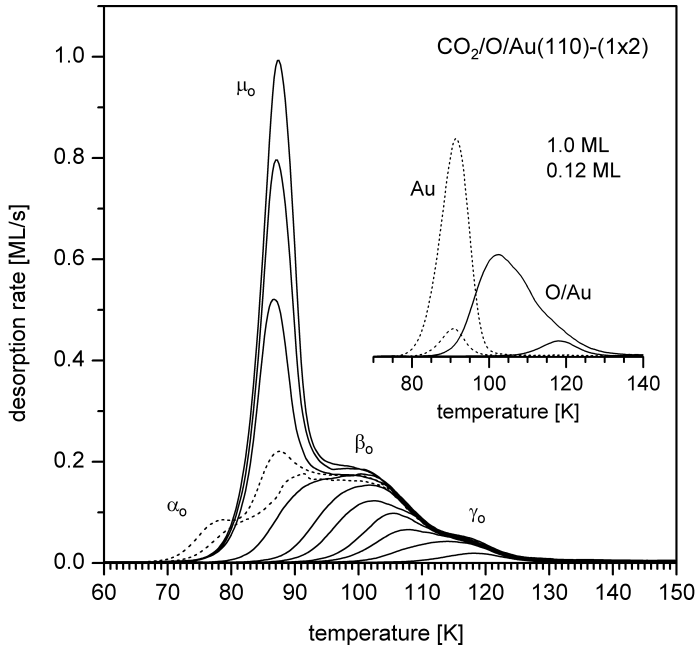


Fig. 10.11: TDS $CO_2$/O/Au(110)-(1×2) for an oxygen precoverage of 1.2 ML. The spectra correspond to the following initial $CO_2$ coverages (in ML): 0.15; 0.30; 0.49; 0.71; 1.00; 1.28; 1.83; 2.08; 2.45; 3.00; 3.75; 4.28. Inset: Desorption spectra from clean and oxygen-precovered Au(110)-(1×2), corresponding to $CO_2$ coverages of 0.12 ML and 1.0 ML. Heating rate 2.45±0.01 K/s for all displayed spectra. $CO_2$ adsorption was carried out at 30 K using a $CO_2$ pressure of $1.38\times10^{-8}$ mbar.

In the sub-monolayer range, we found a correlation between the integrated $\gamma_O$ intensity in the $CO_2$ TDS and the integrated intensity of the gold oxide desorption state $\beta_1$ in the oxygen TDS. We conclude that $\gamma_O$ arises from $CO_2$ which is adsorbed on gold oxide ($\rightarrow$ $\beta_1$-O state), whereas $\beta_2$ stems from adsorption on the chemisorbed oxygen phase ($\beta_2$-O state).

As mentioned above, the low-temperature peak shift suggests $CO_2$-$CO_2$ repulsion in the first layer, which should lead to a desorption energy decrease. However, a leading edge analysis (cf. Section 4.1.3) reveals a complicated interplay between the variations of activation energy and frequency factor, which is difficult to interpret (Fig. 10.12). Initially, $E_{des}$ indeed decreases with increasing coverage. However, above 0.5 ML we find an increase in $E_{des}$ which is overcompensated by a parallel frequency factor increase so that the peak maxima shift further to lower $T_{des}$ despite the increase of $E_{des}$. The low-temperature shift is thus not only a result of the repulsive interactions which reduce the desorption energy (at least not in the whole coverage range), but also due to a growing frequency factor. The latter suggests an adsorbate which is, with growing coverage, increasingly less mobile. This reduced mobility may be connected with the formation of islands.

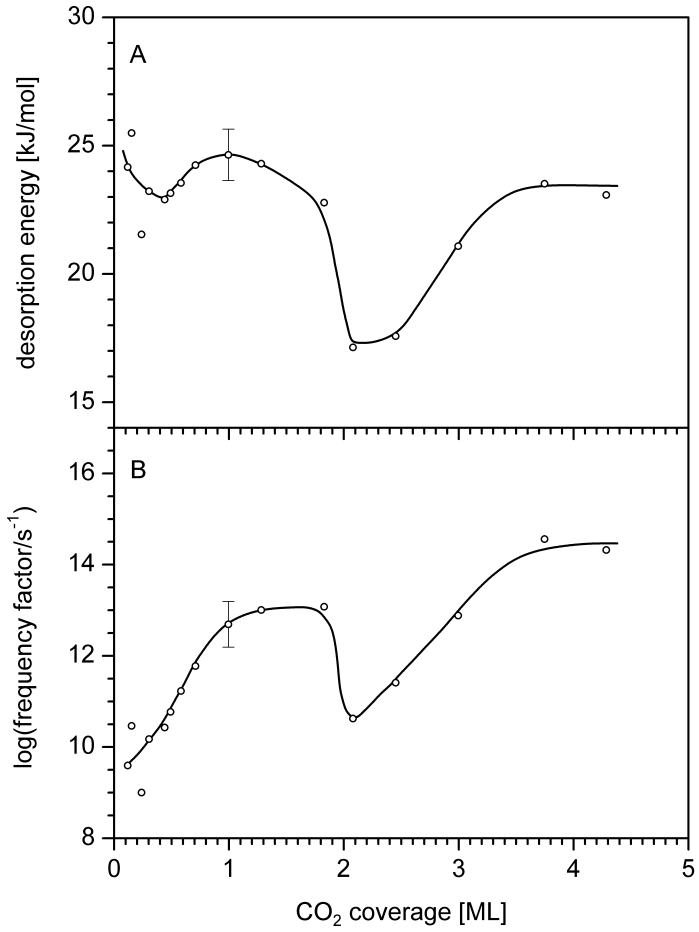


Fig. 10.12: $CO_2$/O/Au(110)-(1×2). Desorption activation energy and log(frequency factor) as functions of coverage, determined by leading edge analysis (cf. Section 4.1.3).

Alternatively, it is also possible to describe the main features of the experimental spectra by assuming a constant ν and a coverage-dependent $E_{des}$. On the basis of this assumption we simulated the thermal desorption spectra by applying the Polanyi-Wigner equation (Eq. 4.1). A comparison of experimental and simulated spectra is shown in Fig. 10.13. The initial desorption energies of $\gamma_O$ and $\beta_O$ are assumed to differ by 0.8 kJ/mol (26.8 and 26.0 kJ/mol, respectively). The best agreement was achieved with a coverage-dependent correction to the initial values of:

$$\Delta E_{des}^{\beta_O} = -4\ \mathrm{kJ/mol} \times \sqrt{\Theta_{\beta_O}} \qquad \text{(Eq. 10.12)for } \beta_O$$

and likewise for $\gamma_O$. A square-root dependence of $E_{des}$ on Θ was also found for the system Xe/Ru(10 $\bar{1}$ 0) [Sc02].

The desorption peak of condensed $CO_2$, $\mu_O$, closely resembles the respective peak for condensed $CO_2$ on the clean surface. Another similarity to the $CO_2$/Au system is the occurrence of a shoulder, here named $\alpha_O$, below the desorption temperature of condensed $CO_2$. We interpret this phenomenon again as caused by desorption of small crystallites which possess a higher Gibbs energy than the infinitely extended condensed phase. The $E_{des}(\Theta)$ diagram in Fig. 10.12 shows that the appearence of $\alpha_O$ is connected with a drop in the desorption energy by ≈ 6 kJ/mol. With Eq. 10.8, we are able to calculate an average crystallite radius of $r_{cryst}$ = 16 Å.

We found no indication for the formation of a stable carbonate species on the gold surface. This result contrasts the findings for $CO_2$ adsorption on O/Ag(110), where carbonate formation has frequently been observed (see, for example, Refs. [Bo80, Gu01]). $CO_3$ on Ag(110) was reported to decompose around 485 K under $CO_2$ release. The remaining O atoms desorb associatively around 590 K [Bo80]. In our experiments, we exposed oxygen-precovered gold to high $CO_2$ dosages (up to 300 L) at temperatures between 28 K and 300 K. Subsequently measured $CO_2$ thermal desorption spectra showed no $CO_2$ desorption between 130 K and the oxygen desorption temperature (< 640 K). Higher carbonate decomposition temperatures can be excluded, because the oxygen TDS confirms the desorption of the complete amount of chemisorbed oxygen, i.e., no oxygen is contained in $CO_3$.

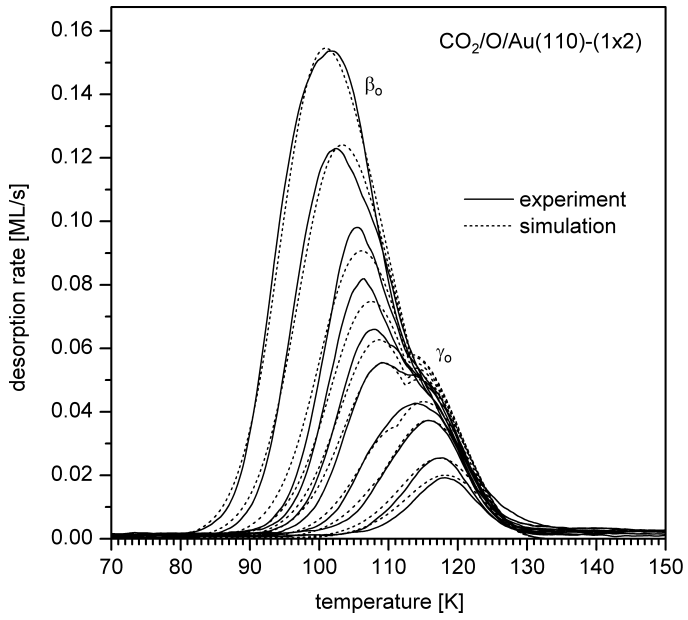


Fig. 10.13: Comparison of experimental (solid lines) and simulated (dotted lines) thermal desorption spectra of $CO_2$/O/Au(110)-(1×2) for an oxygen precoverage of 1.2 ML. Heating rate 2.45±0.01 K/s. The spectra correspond to the following initial $CO_2$ coverages (in ML): 0.12; 0.15; 0.24; 0.30; 0.44; 0.49; 0.58; 0.71; 1.00; 1.28. The simulation was carried out with the following parameters. $\gamma_O$ peak: $E_{des} = (26.8 - 4.0\sqrt{\Theta_{CO2}(\gamma_O)})$ kJ/mol, $\nu = 10^{11}$ s$^{-1}$, n = 1, saturation coverage 0.2 ML. $\beta_O$ peak: $E_{des} = (26 - 4\sqrt{\Theta_{CO2}(\beta_O)})$ kJ/mol, $\nu = 10^{11}$ s$^{-1}$, n = 1. $CO_2$ adsorption was carried out at 30 K and $p(CO_2) = 1.38\times10^{-8}$ mbar.

# 10 Adsorption of carbon dioxide on the clean and on the oxygen-precovered Au(110)-(1×2) surface